Steady-State Rate-Based Simulation of Packed Reactive Distillation: Spatial Discretization

Sebastien Lextrait, R. Bruce Eldridge, and Thomas F. Edgar*

Department of Chemical Engineering, The University of Texas at Austin, Austin, Texas 78712-1062

This paper investigates issues related to the numerical simulation of rate-based models for catalytic distillation processes. Special emphasis is placed on spatial discretization in the solution of steady-state models describing packed reactive distillation columns. A general rate-based model for packed reactive distillation is briefly presented, along with its underlying assumptions. This mathematical model is then discretized along its spatial dimensions using different finite-difference schemes. In this paper, steady-state simulations are considered to assess various properties of the different discretization methods. Using a *tert*-amyl methyl ether (TAME) packed reactive distillation as a case study, we show that a cell-based approach, similarly to a first-order finite-difference approximation, is inefficient in converging to the solution of the mathematical model. To address this problem, a higher-order discretization scheme is used, and its advantages are illustrated. This latter method is of interest for reducing computation time and might permit model-based control strategies, which require steady-state and dynamic models of tractable sizes.

1. Introduction

The application of packed reactive distillation in the chemical processing industry is increasing. Modeling, simulation, analysis, and control of reactive (catalytic) distillation processes are areas of investigation that should be studied in parallel with commercial implementation. The economic optimization and control of packed reactive distillation units require numerical simulations. The variety of mathematical models and the differing performances of numerical methods provide many possible avenues for the investigation, analysis, and control of reactive distillation processes.

The review by Taylor and Krishna[1] provided a general modeling approach for both equilibrium and nonequilibrium (rate-based) models of reactive distillation processes. The macroscopic spatial dimension (column height) in both model types was considered by using a stage or cell approach. For the rate-based modeling of both distillation as well as reactive distillation, Taylor's group published detailed articles that describe the physical assumptions and the model formulation in a general setting,[2−4] although without investigating numerical issues in detail. Kreul et al.[5−7] published a series of contributions that carefully presented several rate-based models for packed reactive distillation. Their approach was similar to that developed by Taylor and Krishna, except that a set of partial differential equations was used instead of a series of cells or stages. The partial differential equations were discretized, and the resulting models were solved using ABACUSS. Issues related to spatial discretization were mentioned, but they were not the main focus of these publications.

This paper focuses on numerical aspects of the simulation of packed reactive distillation columns with rate-based models. We first review the main equations employed for describing the behavior of such a unit, as well as the underlying modeling assumptions. Special emphasis is placed on the numerical solution of the differential-algebraic equations that arise from the material and energy balances along the column length and from the treatment of mass and energy transfer occurring in the liquid and vapor films. The resulting complex nonlinear mathematical model is approximated using several finite-difference schemes to produce discrete models suitable for numerical simulations. A packed reactive distillation column for the production of *tert*-amyl methyl ether (TAME) is used as a case study for analyzing the various finite-difference methods. The validity and use of these approaches are assessed through this example.

2. Mathematical Modeling of Packed Reactive Distillation Columns

Most rate-based models for packed reactive distillation generally arise as extensions of equilibrium models in the sense that the column is viewed as an aggregate of cells of finite volume.[3,8] Within these cells or stages, nonequilibrium processes (mass and energy transfer, chemical reaction) occur. Recently, models that describe the convection in the bulk phases as a mechanism that varies continuously in the spatial position were published.[5,9] In these works, backward differences with respect to the flow direction were applied to discretize the spatial dimension. The resulting models are similar to a nonequilibrium cell-based model.

In this section, a steady-state rate-based model for a general packed reactive distillation column is briefly described, along with its underlying assumptions. We present only the principal equations here; most of the details are included in Appendix A because the equations are available in other references mentioned earlier. Via different numerical techniques that are presented

* To whom correspondence should be addressed. Tel.: +1 (512) 471 3080. Fax: +1 (512) 471 7060. E-mail: edgar@mail.utexas.edu.

10.1021/ie030171n CCC: $27.50
Published on Web 04/16/2004

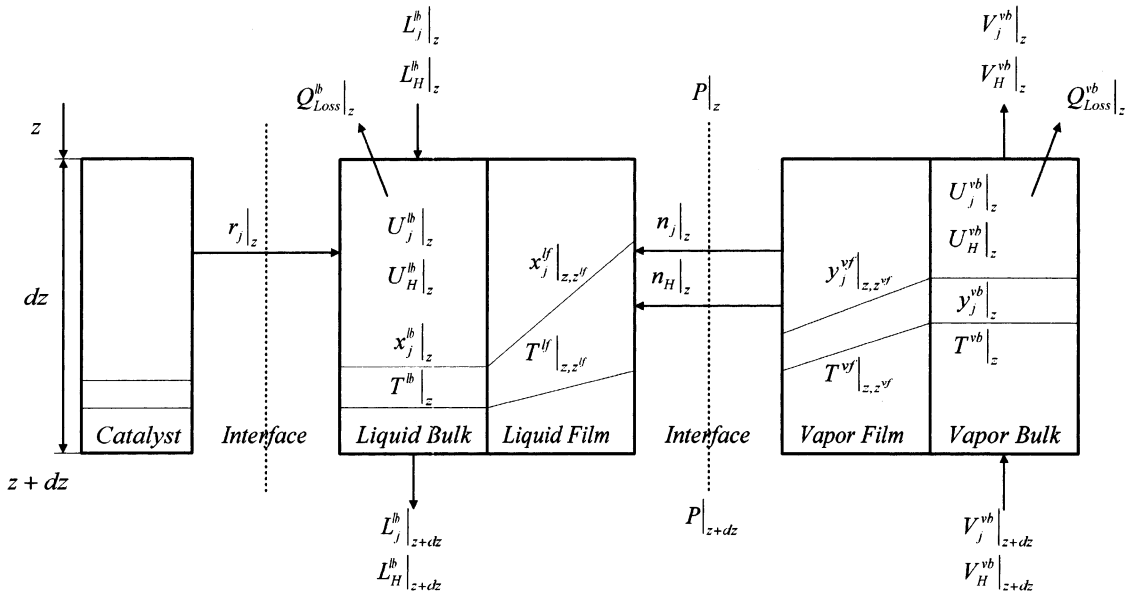

Figure 1. Schematic representation of a two-film interface for a differential packing segment with pseudohomogeneous reactions.

in section 3, the distributed-parameter model is transformed into systems of equations amenable to numerical simulation.

2.1. General Concepts. The standard equipment used for reactive distillation contains reactive and nonreactive sections. The nonreactive sections are identical to the sections traditionally encountered in a packed distillation column, whereas the reactive zone contains a specific catalytic packing that enables chemical reactions to be carried out along with separation. Each of these sections can be mathematically modeled as a set of algebraic equations (AEs) appended to a set of differential equations (DEs). The distributed models for the packed sections are combined with models that describe the auxiliary equipment of the reactive distillation column. The auxiliary models of the column include models for liquid feed distributors, condensers, reflux drums, and reboilers. The resulting steady-state model of the packed reactive distillation process consists of AEs and DEs.

2.2. Packed Sections. The mathematical model of the reactive and nonreactive sections is based on two-film theory.[10] It is assumed that both liquid and vapor bulk phases are ideally mixed and that the mass-transfer resistances are located near the liquid−vapor interface. The chemical reactions are considered to be pseudohomogeneous.[6,7] A schematic representation of a two-film model for a differential packing segment with pseudohomogeneous reactions is shown in Figure 1. The component and energy balances constitute a set of differential equations (eqs 1−4) that describe the macroscopic steady-state behavior of a packed section. The assumption of mechanical equilibrium along the section height is implemented by using an empirical correlation (ΔP) from a steady-state mechanical energy balance (eq 5). The set of equations (eqs 1−5) is a set of balance equations. In any section, there are $2N_{comp} + 3$ differential balance equations. The boundary at the top of a section is taken as the initial value for the spatial dimension. The liquid stream flows down from $z = 0$ to the end of the section ($z = l_s$), while the vapor stream flows up from the end of the section ($z = l_s$) to $z = 0$.

$$-\frac{dL_j^{lb}}{dz} + n_j a_e A_c + r_j \omega_c A_c = 0 \tag{1}$$

$$-\frac{dL_H^{lb}}{dz} + n_H a_e A_c - Q_{Loss}^{lb} = 0 \tag{2}$$

$$\frac{dV_j^{vb}}{dz} - n_j a_e A_c = 0 \tag{3}$$

$$\frac{dV_H^{vb}}{dz} - n_H a_e A_c - Q_{Loss}^{vb} = 0 \tag{4}$$

$$\frac{dP}{dz} - \Delta P = 0 \tag{5}$$

In eqs 1−5, the mass-transfer rates, the energy-transfer rate, the reaction rates, and the pressure drop are unknowns that need to be computed through some mechanism equations. Equation 5 differs from the other equations in the sense that quasi-steady state is assumed for this kind of mechanical energy balance (mechanical equilibrium). The pressure drop correlation (eq 9) is an empirical relation that accounts for the loss in mechanical energy due to friction. The first set of transfer mechanism equations, eqs 6 and 7, provides an explicit representation of the component and energy fluxes across the liquid−vapor interface from the vapor bulk phase to the liquid bulk phase. In fact, these fluxes cannot be computed explicitly because they result from the integration of the Maxwell−Stefan relations in the liquid and vapor films.[10] This issue is described later. The contribution of the chemical reactions and effects of the mass-transfer resistances inside a solid catalyst are modeled using a pseudohomogeneous approach. The different phenomena are lumped together to provide an explicit set of reaction rates (eq 8), which are generally obtained from experi-

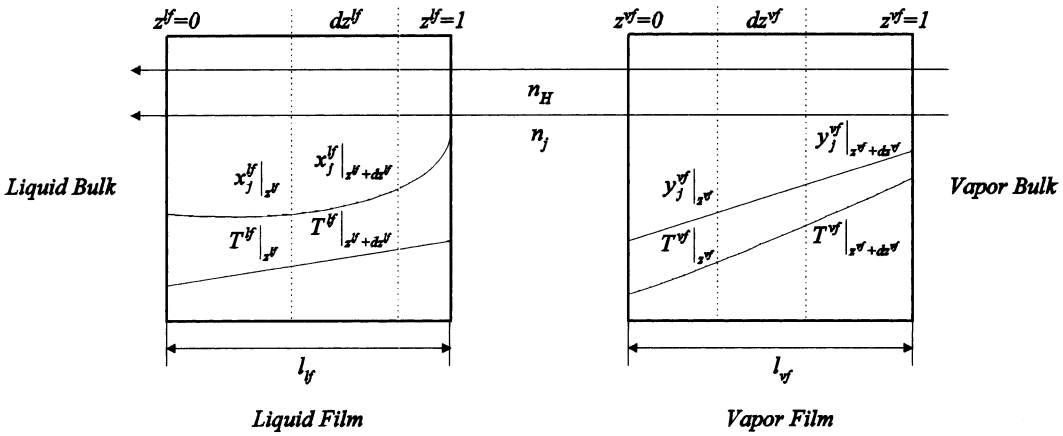

Figure 2. Schematic representation of a liquid−vapor interface.

ments and are considered here as a given kinetics submodel.

$$n_j - f_{j\ \text{molar flux}}(x^{\text{lb}},T^{\text{lb}},\rho^{\text{lb}},\nu^{\text{lb}},L_{\text{T}}^{\text{lb}},y^{\text{vb}},T^{\text{vb}},\rho^{\text{vb}},\nu^{\text{vb}},V_{\text{T}}^{\text{vb}},P,\Phi^{\text{lb}}) = 0 \quad (6)$$

$$n_{\text{H}} - f_{\text{H energy flux}}(x^{\text{lb}},T^{\text{lb}},\rho^{\text{lb}},\nu^{\text{lb}},L_{\text{T}}^{\text{lb}},y^{\text{vb}},T^{\text{vb}},\rho^{\text{vb}},\nu^{\text{vb}},V_{\text{T}}^{\text{vb}},P,\Phi^{\text{lb}}) = 0 \quad (7)$$

$$r_j - f_{j\ \text{molar reaction rate}}(x^{\text{lb}},T^{\text{lb}},L_{\text{T}}^{\text{lb}},\Phi^{\text{lb}}) = 0 \quad (8)$$

$$\Delta P - f_{\text{pressure drop}}(V_{\text{T}}^{\text{vb}},\rho^{\text{vb}},\Phi^{\text{lb}},\nu^{\text{vb}},y^{\text{vb}}) = 0 \quad (9)$$

In addition to the above equations, many equations are required to define intensive potential variables in terms of extensive variables. These equations are sometimes defined as constitutive relationships (see Appendix A).

The algebraic and differential equations need to be completed with boundary conditions. The boundary conditions define the flow rates of material and energy entering the section as well as the pressure at the top ($z = 0$) of the packed section. The boundary condition that is related to the liquid bulk phase is specified at $z = 0$ by setting the rates of material and energy flowing through the boundary, whereas the boundary related to the vapor phase is given at $z = l_s$.

2.3. Maxwell−Stefan Relations. Equations 6 and 7 in the mathematical model for the packed sections is discussed further here. The material and energy fluxes across the liquid−vapor interface are computed through the integration of the Maxwell−Stefan relations in both films (mesoscopic scale). However, any consistent submodel that determines fluxes crossing the interface can be used. When Maxwell−Stefan equations are used, the mathematical submodel describing the mechanisms inside the interface (liquid film, interface, and vapor film) consists of algebraic and differential equations. The phenomena occurring between the two bulk phases are idealized in the two-film theory framework.[10] An idealized representation of the liquid−vapor interface is shown in Figure 2. The generalized Maxwell−Stefan relations relate the fluxes to the driving forces, as specified in eqs 10−15.

$$d_j^{\text{lf}} - \sum_{k=1}^{N_{\text{comp}}} \frac{x_k n_j - x_j n_k}{\rho^{\text{lf}} Đ_{j,k}^{\text{lf}}} = 0 \quad (10)$$

$$d_j^{\text{vf}} - \sum_{k=1}^{N_{\text{comp}}} \frac{y_k n_j - y_j n_k}{\rho^{\text{vf}} Đ_{j,k}^{\text{vf}}} = 0 \quad (11)$$

$$d_j^{\text{lf}} - \sum_{k=1}^{N_{\text{comp}}} \frac{x_k n_j - x_j n_k}{\rho^{\text{lf}} \kappa_{j,k}^{\text{lf}}} = 0 \quad (12)$$

$$d_j^{\text{vf}} - \sum_{k=1}^{N_{\text{comp}}} \frac{y_k n_j - y_j n_k}{\rho^{\text{vf}} \kappa_{j,k}^{\text{vf}}} = 0 \quad (13)$$

$$\sum_{k=1}^{N_{\text{comp}}} \frac{\text{d}x_k^{\text{lf}}}{\text{d}z^{\text{lf}}} = 0 \quad (14)$$

$$\sum_{k=1}^{N_{\text{comp}}} \frac{\text{d}y_k^{\text{vf}}}{\text{d}z^{\text{vf}}} = 0 \quad (15)$$

Equations 10 and 11 are integrated along the two film lengths. Only $N_{\text{comp}} - 1$ of these relations are independent in each film, and the mole fractions are required sum to unity. A problem that one encounters when solving the Maxwell−Stefan equations is the lack of knowledge regarding the film lengths. Different approaches have been proposed to solve this problem. Taylor and Krishna reformulated the equations in terms of binary mass-transfer coefficients that are evaluated through some empirical correlations[10] that express the binary mass-transfer coefficients as a function of the Maxwell−Stefan diffusivities, the packing characteristics, and the operating conditions. These relations are the so-called Sherwood or mass-transfer correlations. Because eqs 10 and 11 are not part of the mathematical model, they are replaced by eqs 12 and 13, which relate the fluxes to dimensionless driving forces (d_j). Because $N_{\text{comp}} - 1$ of these dimensionless equations are independent, relations 14 and 15 are required.

The energy flux is defined by eqs 16 and 17: one relation for each film. Two phenomena contribute to the energy transfer across the interface, which is both a conductive process and a diffusive process.

$$n_{\mathrm{H}} - h^{\mathrm{lf}}\frac{\mathrm{d}T^{\mathrm{lf}}}{\mathrm{d}z^{\mathrm{lf}}} - \sum_{k=1}^{N_{\mathrm{comp}}} n_k H_k^{\mathrm{lf}} = 0 \tag{16}$$

$$n_{\mathrm{H}} - h^{\mathrm{vf}}\frac{\mathrm{d}T^{\mathrm{vf}}}{\mathrm{d}z^{\mathrm{vf}}} - \sum_{k=1}^{N_{\mathrm{comp}}} n_k H_k^{\mathrm{vf}} = 0 \tag{17}$$

The (dimensionless) driving forces that are functions of chemical potential gradients and other variables can be expressed, in a general setting, as explicit functionals of mole fraction gradients, mole fractions, and temperature (eqs 18 and 19). These general relations depend on the modeling assumptions. For the simplest case (ideal phase), the dimensionless driving forces are reduced to the mole fraction gradients. For a nonideal mixture, these equations involve the computation of correction terms to account for the nonidealities.[10]

$$d_j^{\mathrm{lf}} - f_{j\ \text{liquid driving force}}\left(\frac{\mathrm{d}x^{\mathrm{lf}}}{\mathrm{d}z^{\mathrm{lf}}}, x^{\mathrm{lf}}, T^{\mathrm{lf}}\right) = 0 \tag{18}$$

$$d_j^{\mathrm{vf}} - f_{j\ \text{vapor driving force}}\left(\frac{\mathrm{d}y^{\mathrm{vf}}}{\mathrm{d}z^{\mathrm{vf}}}, y^{\mathrm{vf}}, T^{\mathrm{vf}}\right) = 0 \tag{19}$$

The preceding equations used for describing the liquid−vapor interface are completed with boundary conditions. In the liquid film, at $z^{\mathrm{lf}} = 0$, the mole fractions are equal to the mole fractions of the liquid bulk phase. The temperature behaves in a similar manner. In the vapor film, at $z^{\mathrm{vf}} = 1$, the bulk and film vapor mole fractions are equal, as are the vapor temperatures. Moreover, some of the physical properties computed in the interface submodel require variables of the bulk phases. This is the case for the mass-transfer and heat-transfer coefficients, which are evaluated through empirical correlations that depend on macroscopic properties. True boundary conditions exist at the liquid−vapor interface, i.e., phase equilibrium is assumed (eqs 20−22).

$$K_j - f_{j\ \text{equilibrium constant}}(x^{\mathrm{lf}}|_{z^{\mathrm{lf}}=1}, y^{\mathrm{vf}}|_{z^{\mathrm{vf}}=0}, T^{\mathrm{lf}}|_{z^{\mathrm{lf}}=1}, P) = 0 \tag{20}$$

$$y_j^{\mathrm{vf}}|_{z^{\mathrm{vf}}=0} - K_j x_j^{\mathrm{lf}}|_{z^{\mathrm{lf}}=1} = 0 \tag{21}$$

$$T^{\mathrm{vf}}|_{z^{\mathrm{vf}}} = 0 - T^{\mathrm{lf}}|_{z^{\mathrm{lf}}=1} = 0 \tag{22}$$

In Appendix A, a set of algebraic relations that describe physical and thermodynamic properties used in the liquid−vapor interface submodel is presented for completeness.

2.4. Auxiliary Equipment. A packed reactive distillation unit consists of the column and some auxiliary equipment, which usually includes a condenser, a reboiler, a reflux drum, pipes, pumps, and control devices. Different approaches exist for modeling these parts of the process, depending on the assumptions being made. To formulate a consistent mathematical model for these pieces of equipment, careful modeling is required. The resulting mathematical models are systems of algebraic equations, which are appended to the equations that describe the column to constitute an overall process model.

2.4.1. Condenser. The condenser is a subcooled vessel that contains an inert component that is found only at the top of the column. Inside the condenser, liquid−vapor phase equilibrium is assumed. Overall material and energy balances define a set of $N_{\mathrm{comp}} + 2$ equations (eqs 23−25). The inert material is present only in the vapor phase. Two vapor streams enter the condenser: one comes from the top of the column and the other comes from the reflux drum. A vapor stream and a liquid stream, connected to the reflux drum, exit the condenser.

$$V_j^{\text{Column}} + V_j^{\text{Reflux drum}} - L_j^{\text{Condenser}} - V_j^{\text{Condenser}} = 0 \tag{23}$$

$$V_{\text{Inert}}^{\text{Reflux drum}} - V_{\text{Inert}}^{\text{Condenser}} = 0 \tag{24}$$

$$V_{\mathrm{H}}^{\text{Column}} + V_{\mathrm{H}}^{\text{Reflux drum}} - L_{\mathrm{H}}^{\text{Condenser}} - V_{\mathrm{H}}^{\text{Condenser}} - Q_{\mathrm{C}} - Q_{\text{Loss}}^{\mathrm{T}} = 0 \tag{25}$$

The liquid and vapor bulk phases are defined through algebraic equations, which are found in Appendix A. These relations are the well-known equations used in equilibrium stages. The liquid material and energy holdups are paired with equations defining the total material and energy holdups. The liquid mole fractions are computed through relations that define the liquid molar holdups, and the liquid enthalpy is obtained by an equation that specifies the liquid energy holdup. The liquid temperature is implicitly determined through a liquid enthalpy model. The liquid flow rate of the stream leaving the condenser is obtained by a Bernoulli-type relation. The vapor bulk phase is determined through a set of equations that are similar in structure to those used in defining the liquid bulk phase. However, the symmetry between liquid and vapor phases that exists in the mathematical models of the packed sections is lost upon the assumption of liquid−vapor equilibrium. In the proposed condenser model, the cooling duty, Q_{C}, is fixed as an operating parameter. A different condenser configuration is possible for steady-state simulation: instead of fixing the cooling duty, the temperature of the condenser can be specified.

2.4.2. Reboiler. The mathematical model for the reboiler is similar to that for the condenser, with minor modifications. No inert component is present, and the cooling duty is replaced by heat duty. To define the steady-state behavior of the reboiler, an extensive variable (liquid volume, total molar holdup, etc.) and an operating parameter (heat duty, bottoms flow rate) need to be fixed.

2.4.3. Reflux Drum. The reflux drum is a vessel that receives streams from the condenser (liquid and vapor) and from an inert source. It has two liquid outlets (reflux and distillate) and a vent for the vapor phase. In the reflux drum, no mass or energy transfer between the two phases occurs, because of the small contact area. Therefore, material and energy balances are written for each phase (eqs 26−30).

$$L_j^{\text{Condenser}} - L_j^{\text{Distillate}} - L_j^{\text{Reflux}} = 0 \quad (26)$$

$$L_{\text{H}}^{\text{Condenser}} - L_{\text{H}}^{\text{Distillate}} - L_{\text{H}}^{\text{Reflux}} - Q_{\text{Loss}}^{\text{L}} = 0 \quad (27)$$

$$V_j^{\text{Condenser}} - V_j^{\text{Reflux drum}} - V_j^{\text{Vent}} = 0 \quad (28)$$

$$V_{\text{Inert}}^{\text{Condenser}} + V^{\text{Inert}} - V_{\text{Inert}}^{\text{Reflux drum}} - V^{\text{Vent}}_{\text{Inert}} = 0 \quad (29)$$

$$V_{\text{H}}^{\text{Condenser}} + V_{\text{H}}^{\text{Inert}} - V_{\text{H}}^{\text{Reflux drum}} - V_{\text{H}}^{\text{Vent}} - Q_{\text{Loss}}^{\text{V}} = 0 \quad (30)$$

In the reflux drum, there are several degrees of freedom, thus allowing some operating conditions to be stipulated. The steady-state behavior of the reflux drum can be specified in various ways. In one approach, the pressure, the reflux ratio, and the total liquid molar holdup can be set, which is usually well-suited for numerical simulation. A second approach, which relates to the physical mechanisms occurring in the reflux drum, fixes the opening percentage of the vent valve and the inert inlet flow rate instead of setting the pressure. The complete set of equations used in modeling the reflux drum is presented in Appendix A.

3. Spatial Discretization

A mathematical model of a packed reactive distillation process that is built using the steady-state submodels briefly presented in the preceding section is a complex set of nonlinear algebraic and differential equations that need to be solved numerically. Here, the spatial derivatives of the mathematical model are approximated using different finite-difference schemes to describe the dependence of the solution as a function of the spatial dimension. To assess the different methods, steady-state solutions are solved. First, an overview of the possible numerical approximations is presented, and then two particular approaches are investigated.

Distributed-parameter models for chemical processes are usually approximated to be solved numerically. When models include spatial dimensions, which occurs in distributed-parameter systems, some discretization techniques are applied to approximate the spatial behavior. Possible techniques for achieving this goal include the finite-difference method, the finite-element method, and the method of weighted residuals. The dependence on the spatial dimensions is expressed by algebraic relations. The general mathematical model is then transformed into a set of algebraic equations (material and energy balances) plus possibly some algebraic equations that result from the different spatial discretization methods. Solution techniques are well-known and have been used for many years in different engineering fields. The method of weighted residuals was extensively studied by Finlayson.[11] It encompasses several methods (collocation, Galerkin, integral, etc.) and is relatively easy to apply.

The finite-difference method was chosen here for approximating the spatial dependence because of its intuitive characteristics, its simple implementation, the nature of the boundary conditions, and the regular geometry of the problem. The general structure of the discrete models obtained from finite-difference approaches is very similar to that of cell-based models. The physical meaning and the variable−equation pairings are unchanged. The structure of the resulting system of AEs is transparent. Although the finite-element method can produce a discrete model with better numerical properties, the appealing structure of the Jacobian matrices is lost for chemical engineering problems with recycle streams. Therefore, the finite-difference method was chosen.

3.1. Cell-Based Approach. The cell-based approach has been used extensively for modeling many chemical processes that are intrinsically distributed-parameter systems. For example, plug-flow reactors are sometimes described by a series of continuous stirred tanks, and membrane separation is viewed a sequence of perfectly mixed units of finite volume connected in series. This approach is relevant when, in addition to the convection process occurring along the macroscopic dimension of the process (reactor length, column height), mesoscopic phenomena (reaction, mass transfer) contribute moderately. Nevertheless, when many rate-based mechanisms occur in addition to convection, the resulting mass and energy balances become more complex. Using a cell-based approach, which is a kind of first-order finite-difference approximation, can be inefficient and misleading. Convergence to the solution of the distributed model requires a large number of discretization points (sometimes several hundreds) when the rates of two (or more) rate-based mechanisms are of different orders of magnitude or extremely nonlinear and vary greatly along the macroscopic dimension of the process. Also, the operating conditions significantly influence the accuracy of the approximation. Indeed, a process operating far from equilibrium, i.e., with operative rate-based mechanisms, requires a large number of discretization points to effectively account for the wide variability and activity of the rate-based mechanisms. Packed reactive distillation columns are among these processes that can require excessive discretization points and are poorly approximated when a cell-based approach is employed.

The numerical implementation of a cell-based model is simple and intuitive. The grid used for discretizing the differential equations along the section lengths is shown in Figure 3. It is usually a grid of constant mesh size. In a cell-based model with N gridblocks, eqs 1−5 are transformed into N sets of equations, while the set of algebraic equations arising from constitutive relations and discretization of the liquid−vapor transfer mechanisms is computed N times, once for each gridblock. A cell-based approach is not exactly a traditional first-order finite-difference approximation of the mathematical model; it is a first-order backward-difference approximation along the flow direction. Therefore, the liquid and vapor bulk phases are discretized unevenly. The following convention determines how the mathematical model is discretized. For gridblock i, any variable that represents a property of the liquid phase is replaced by its values at $z_{i+1/2} = \sum_{k=1}^{i} \Delta z_k$, whereas for the vapor phase, the discrete approximation uses the value of the variable at $z_{i-1/2} = \sum_{k=1}^{i-1} \Delta z_k$. The spatial derivatives are approximated as shown in eqs 31−32. The liquid

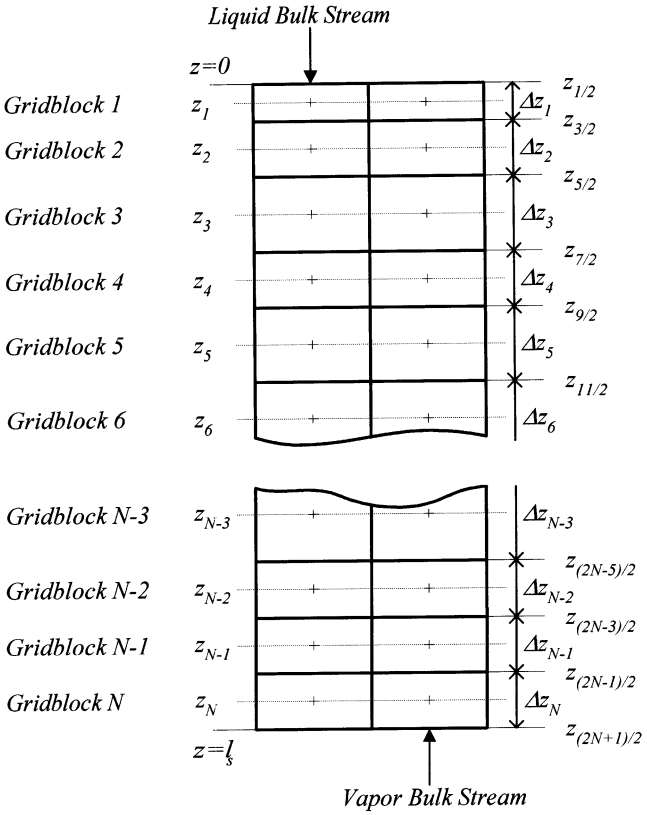

Figure 3. Schematic representation of the grid for spatial discretization along column height.

and vapor spatial derivative approximations are similar.

$$\left.\frac{dL_j^{lb}}{dz}\right|_i = \frac{L_j^{lb}\big|_i - L_j^{lb}\big|_{i-1}}{\Delta z_i} = \frac{L_j^{lb}\Big|_{(z_{i+1/2}=\sum_{k=1}^{i}\Delta z_k)} - L_j^{lb}\Big|_{(z_{i-1/2}=\sum_{k=1}^{i-1}\Delta z_k)}}{\Delta z_i} \quad (31)$$

$$\left.\frac{dV_j^{lb}}{dz}\right|_i = \frac{V_j^{lb}\big|_{i+1} - V_j^{lb}\big|_i}{\Delta z_i} = \frac{V_j^{lb}\Big|_{(z_{i+1/2}=\sum_{k=1}^{i}\Delta z_k)} - V_j^{lb}\Big|_{(z_{i-1/2}=\sum_{k=1}^{i-1}\Delta z_k)}}{\Delta z_i} \quad (32)$$

As can be seen in the above equations, the cell-based model has an awkward symmetry. The discrete variables used in a given gridblock i are located at different positions depending on the phase being described. A shift of Δz_i occurs between the locations of the liquid-related variables and those of the corresponding vapor-related variables. Thus, material and energy fluxes evaluated through relations requiring variables from both phases poorly approximate the mass and energy transfer for gridblock i. A similar problem is encountered in approximating the contributions of the chemical reactions. Indeed, for gridblock i, the discrete values of the reaction rates are evaluated at the bottom of the gridblock at $z_{i+1/2} = \sum_{k=1}^{i}\Delta z_k$. This creates a shift of $\Delta z_i/2$ in the location that is used to approximate the reaction rates for gridblock i, which is a weakness of the traditional cell-based approach.

These remarks point out some of the weaknesses of the traditional cell-based models. If a numerical solution of the distributed model is sought, it is likely that such an approach will perform poorly. A cell-based model requires a large number of cells to decrease the effects of the above-mentioned shifts in location so that the discrete material and energy balances truly describe the physical behavior inside a given gridblock. For these reasons, an improved numerical technique, a higher-order finite-difference scheme, is investigated here.

3.2. Higher-Order Schemes. The cell-based approach presented in the preceding section contains certain approximation properties that need to be improved. The main shortcomings are in the approximations of rate processes inside gridblocks. For example, the material and energy fluxes are evaluated for the liquid and vapor bulk phases at points separated by a distance of Δz_i. A higher-order scheme discrete model is able to alleviate these difficulties.[12,13] For gridblock i, the equations are evaluated at the gridblock center located at $z_i = \sum_{k=1}^{i-1}\Delta z_k + \Delta z_i/2$. The discrete approximations of the differential equations, the algebraic equations for both phases, and the algebraic equations arising from the discretization of the liquid−vapor interface submodel are evaluated at z_i. To implement this approximation method, a slightly modified grid, as shown in Figure 3, is required. Some variables and equations are added to the discrete model. Variables representing the material and energy flow rates in both phases, as well as the pressure on the edges of the gridblocks, are defined. These variables, located at $z_{i+1/2} = \sum_{k=1}^{i}\Delta z_k$, $i = 0, ..., N$, constitute a set of $(N + 1)(2N_{comp} + 3)$ variables that support the computations and are used for finite-difference approximations of properties located at z_i. The equations associated with these variables include $N(2N_{comp} + 3)$ finite-difference relations and $2N_{comp} + 3$ boundary conditions. For each gridblock i, the finite-difference equations relate a variable $C|_{z=z_i}$ located at z_i, to four variables $C|_{z=z_{i+l+1/2}}$, $l \in \{-3, -2, -1, 0, 1, 2\}$, located on the edge of the gridblocks.

The material and energy flow rates and the pressure variables located at $z_i = \sum_{k=1}^{i-1}\Delta z_k + \Delta z_i/2$, $i = 1, ..., N$, are used to approximate and evaluate the chemical processes that occur inside each gridblock. The derivatives with respect to the spatial dimension of the liquid and vapor material and energy flow rates are evaluated, in each gridblock, by higher-order finite-difference approximations. The variables located at z_i, which represent the majority of the variables of the model, are determined by algebraic equations (constitutive relations, discretization of the liquid−vapor transfer mechanisms) and evaluated N times, once for each gridblock. The derivatives of the variables at z_i are evaluated through some formulas similar to the ones used to relate the variable $C|_{z=z_i}$ to a linear combination of four variables $C|_{z=z_{i+l+1/2}}$, $l \in \{-3, -2, -1, 0, 1, 2\}$, located on the edge of the gridblocks. The same approach for computing these approximations is employed. The variables or the spatial derivatives of the variables to be approximated are expressed through linear combinations of four variables located at $z_{i+l+1/2}$, $l \in \{-3, -2, -1, 0, 1, 2\}$. The coefficients of the linear combinations are computed using a Taylor series expansion and grid setting, according to eqs 33 and 34.

$$\begin{bmatrix} 1 & 1 & 1 & 1 \\ d_{a\to z} & d_{b\to z} & d_{c\to z} & d_{d\to z} \\ d_{a\to z}^{\,2} & d_{b\to z}^{\,2} & d_{c\to z}^{\,2} & d_{d\to z}^{\,2} \\ d_{a\to z}^{\,3} & d_{b\to z}^{\,3} & d_{c\to z}^{\,3} & d_{d\to z}^{\,3} \end{bmatrix} \begin{bmatrix} \alpha_z \\ \beta_z \\ \gamma_z \\ \delta_z \end{bmatrix} = \begin{bmatrix} 1 \\ 0 \\ 0 \\ 0 \end{bmatrix} \tag{33}$$

$$\begin{bmatrix} 1 & 1 & 1 & 1 \\ d_{a\to z} & d_{b\to z} & d_{c\to z} & d_{d\to z} \\ d_{a\to z}^{\,2} & d_{b\to z}^{\,2} & d_{c\to z}^{\,2} & d_{d\to z}^{\,2} \\ d_{a\to z}^{\,3} & d_{b\to z}^{\,3} & d_{c\to z}^{\,3} & d_{d\to z}^{\,3} \end{bmatrix} \begin{bmatrix} \alpha'_z \\ \beta'_z \\ \gamma'_z \\ \delta'_z \end{bmatrix} = \begin{bmatrix} 0 \\ 1 \\ 0 \\ 0 \end{bmatrix} \tag{34}$$

The coefficients α_z, β_z, γ_z, and δ_z define a linear combination that relates a variable C located at z to four values of the variable located at the four positions $z + d_{a\to z}$, $z + d_{b\to z}$, $z + d_{c\to z}$, $z + d_{d\to z}$, as shown in eq 35. The values of the displacement parameters ($d_{a\to z}$, $d_{b\to z}$, $d_{c\to z}$, $d_{d\to z}$) depend on the gridblock for which the approximation is being made. The spatial derivative $(\mathrm{d}C/\mathrm{d}z)|_z$ is approximated in a similar fashion, as shown in eq 36.

$$C|_z = \alpha_z C|_{z+d_{a\to z}} + \beta_z C|_{z+d_{b\to z}} + \gamma_z C|_{z+d_{c\to z}} + \delta_z C|_{z+d_{d\to z}} \tag{35}$$

$$\left.\frac{\mathrm{d}C}{\mathrm{d}z}\right|_z = \alpha'_z C|_{z+d_{a\to z}} + \beta'_z C|_{z+d_{b\to z}} + \gamma'_z C|_{z+d_{c\to z}} + \delta'_z C|_{z+d_{d\to z}} \tag{36}$$

The higher-order scheme has an order of accuracy of $O(\Delta z^3)$ for the first derivative and $O(\Delta z^4)$ for the variable itself. A grid of N gridblocks is defined, and then the displacement parameters are evaluated. For gridblock 1, the displacement parameters are given by $-\Delta z_1/2$, $\Delta z_1/2$, $\Delta z_1/2 + \Delta z_2$, and $\Delta z_1/2 + \Delta z_2 + \Delta z_3$. Also, the displacement parameters of the last gridblock are defined by $-\Delta z_N/2 - \Delta z_{N-1} - \Delta z_{N-2}$, $-\Delta z_N/2 - \Delta z_{N-1}$, $-\Delta z_N/2$, and $\Delta z_N/2$. The remaining displacement parameters for gridblock i, $i = 2, \ldots, N-1$, are given by the general expressions $-\Delta z_i/2 - \Delta z_{i-1}$, $-\Delta z_i/2$, $\Delta z_i/2$, and $\Delta z_i/2 + \Delta z_{i+1}$. Once the displacement parameters are defined, the weights of the linear combinations are evaluated by eqs 33 and 34.

To numerically solve the differential equations of the liquid−vapor interface submodel, the same higher-order scheme is used. Two grids, one for each film, are defined and the numerical approximations are carried out. The algebraic and differential equations are evaluated within each gridblock. This leads to $N_{\mathrm{lfm}} + N_{\mathrm{vfm}}$ sets of equations that consist of algebraic equations evaluated at the center of each gridblock. Among these equations, the discrete equivalents of the differential equations are present.

3.3. Numerical Implementation. Each of the two methods, namely, the cell-based approach and the higher-order scheme, transforms the mathematical model into a system of algebraic equations. The liquid−vapor interface submodel is discretized, and its equations and variables are added to the model of the packed section. In a discrete model of a packed section, the spatial dependence is cast into N discrete sets of algebraic equations.

The modeling of packed reactive distillation processes considered here is oriented toward model-based control or optimization-related issues. Therefore, the models studied were developed in a general flexible framework to be integrated with control and optimization software. The models were coded in Fortran. The procedure to build a process model is an "object-oriented" one. The problem configuration is defined through some input files, and the overall process model, with its structure, equations, and other properties, is built sequentially, one physical unit after another. The resulting overall model made of appended submodels is then created. It consists of the appended variables and residuals of each submodel coded in Fortran.

In building and solving the overall process model, different tasks are performed. For each of these tasks, the mathematical submodels have their own set of subroutines, which carry out each of these tasks individually. An overall schematic representation of the numerical implementation is shown in Figure 4. Basically, the different tasks are initialization, sparsity pattern determination, residual evaluation, and Jacobian evaluation. The initialization procedure, by sequentially calling the initialization subroutines of the different submodels, defines the variable names, residual names, variable bounds, initial variable values, and variable and function scaling parameters for the overall process model. The second task determines the sparsity pattern of the Jacobian matrix of the overall process model. This procedure calls the sparsity pattern subroutines of the submodels used in the overall process model. Then, in solving the overall process model, the residuals and the Jacobian matrix are evaluated. These two tasks are effected by calling individual subroutines for each submodel. The overall process model is built in an object-oriented fashion because it is an aggregate of submodels. Each subroutine takes pointer positions of variables and residuals to be used in the submodel. The variables of a given submodel are supplied to any subroutine via pointers. However, the solution procedure of the overall resulting model is "equation-oriented" because the equations are solved at one time.

The approach used in solving the discrete models converts the mathematical model into a set of nonlinear algebraic equations. This set of equations is solved using a nonlinear programming (NLP) software package named NOVA (nonlinear optimization for versatile applications) and developed by Dot Products (www.dot-products.com).

The main difficulty encountered in developing this simulation environment is related to the proper use of pointers for building an overall discrete process model. Extreme care has been used in creating a flexible environment in which the packed reactive distillation column configuration is described by data stored in external input files. The subroutines of the submodels are "objects" that take only pointers and a vector containing all of the variables of the overall model, as well as some parameters. This approach makes the process model easy to change when different submodels are to be employed. In addition to designing a systematic flexible modeling environment, different techniques to ease the numerical solution of the resulting nonlinear sets of algebraic equations have been incorporated. The key idea is to generate and solve a sequence of discrete models of increasing complexity. The procedure is automated: First, the complexity is increased in the physical description of the chemical processes occurring in the column (from equilibrium to rate-based) and then the spatial discretization is refined (number of gridblocks, method of discretization). Continuation methods[14] are employed to solve models of increasing com-

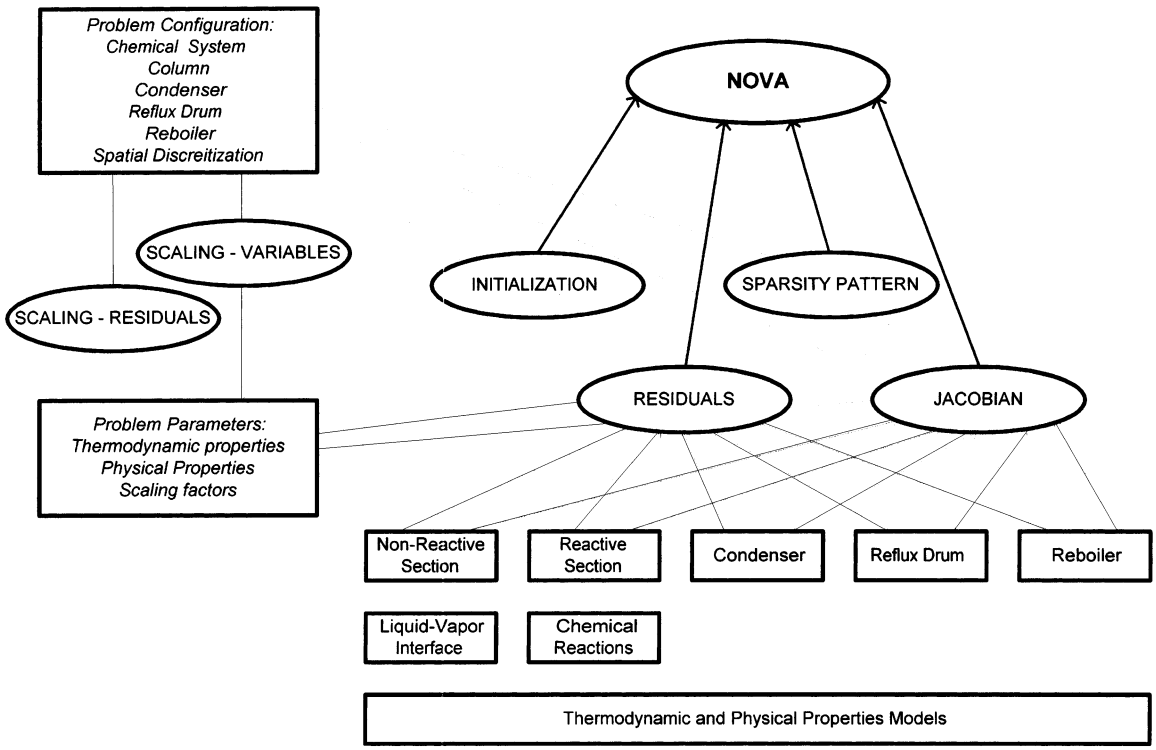

Figure 4. Schematic representation of the numerical implementation.

plexity in terms of physical description. The rate processes (material and energy fluxes and reaction rates) and the reflux ratio have significant effects on the complexity of the models. These variables are multiplied by some continuation parameters, allowing solution of models of increasing complexity to be achieved. The refinement of the spatial discretization generates initial guesses for the more refined models by linear interpolation. Once a steady-state solution for a discrete model is obtained, new solutions for this discrete model, under different operating conditions, are obtained easily without requiring any of the techniques mentioned above (sequential solution of models of increasing complexity, continuation) to be re-executed. These methods are required only to generate a solution for a complex model or to switch from a nominal model to a more refined one.

4. Application to a TAME-Packed Reactive Distillation Column

In this section, a packed reactive distillation column for the production of TAME is modeled and simulated using the general framework presented earlier. Steady-state profiles are obtained and compared to assess the performance characteristics of the finite-difference schemes. The set of algebraic equations is solved using NOVA for different spatial discretization configurations. The results are valid for the TAME column under specified operating conditions. Nevertheless, these findings should be relevant when other packed reactive distillation processes are investigated. Numerical simulations of a packed reactive distillation unit can exhibit very different characteristics. As the spatial discretization is refined, the solution of the discrete model varies. Once the spatial discretization configuration is sufficiently refined, the discrete model has converged to the solution of the distributed-parameter model. In any event, experimental data are required to validate the mathematical model, which is numerically solved under an appropriate level of spatial discretization.

The TAME process under study is a packed reactive distillation pilot plant built at the Separations Research Program (SRP) facility, University of Texas, Austin, TX. The column configuration is shown in Figure 5. The configuration parameters and the operating conditions used in the simulations are reported in Table 1. The chemical system is modeled using five components: methanol, 2-methyl-1-butene (2M1B), 2-methyl-2-butene (2M2B), *tert*-amyl methyl ether (TAME), and *n*-pentane. The UNIQUAC model is used to evaluate the liquid activity coefficients. The kinetic model developed by Rihko et al.[15,16] accounts for the chemical reactions as well as the internal catalyst mass-transfer resistances. To compute the pressure drop, the specific effective liquid−vapor interfacial area, and the liquid volume fraction, a model for structured packings is used.[17,18] The remaining physical, chemical, and thermodynamic property methods employed in this work are described in Appendix B.

Different spatial discretization configurations are used to investigate the performance of the cell-based and higher-order schemes. The main contribution of this paper is to show how poorly a cell-based model performs when one intends to obtain a numerical solution of the distributed mathematical model and how a higher-order scheme can alleviate this difficulty. A numerical solution of the distributed mathematical model is often sought and assumed to be attained when a sufficiently refined block size is used. For example, this goal is implicitly mentioned by Baur et al. when they write: "Our study shows that at least 90 slices are required for acceptable accuracy. Increasing the number of slices beyond 90 does not alter the results."[2] Kreul also states: "Segment heights smaller than 12.5 cm (HETP/2) showed no additional influence on the solution except extending the need for CPU time."[7] However, rarely are details

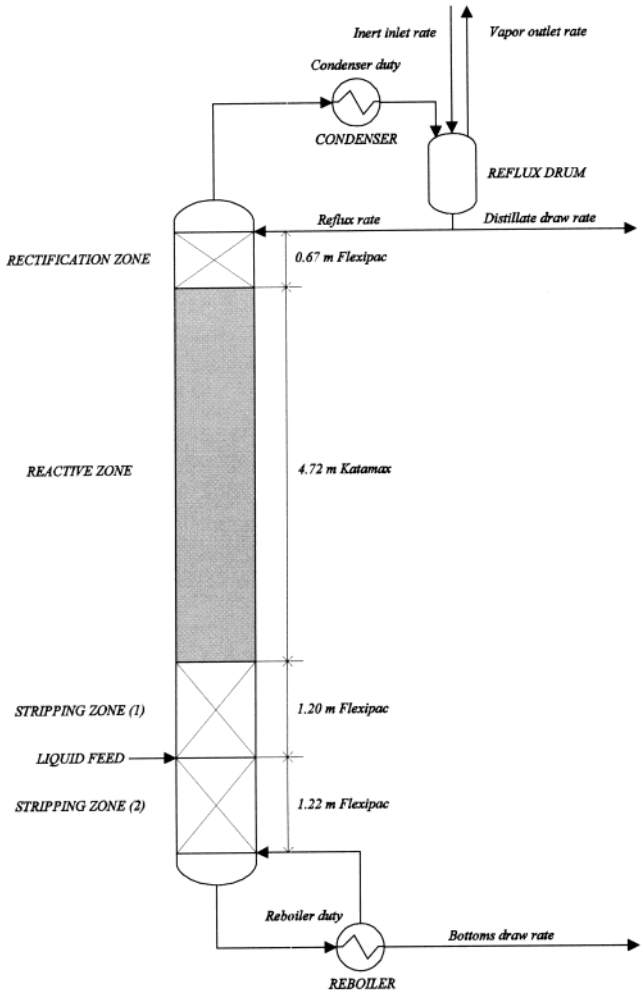

Figure 5. Pilot-plant packed reactive distillation column at SRP.

Table 1. Column Configuration and Operating Conditions for the TAME System

variable	value
length rectification zone	0.67 m
length reactive zone	4.72 m
length stripping zone (1)	1.20 m
length stripping zone (2)	1.22 m
column diameter	1.6150×10^{-1} m
condenser volume	1.5×10^{-2} m^3
reflux drum volume	4.0×10^{-2} m^3
reboiler volume	8.0×10^{-2} m^3
condenser pressure	3.8×10^{5} Pa
condenser temperature	342.15 K
reflux ratio	3.0 (none)
bottoms flow rate	4.2027×10^{-5} kmol/s
feed flow rate	3.0025×10^{-4} kmol/s
feed methanol mole fraction	2.5988×10^{-1}
feed 2M1B mole fraction	7.3508×10^{-3}
feed 2M2B mole fraction	7.1013×10^{-2}
feed TAME mole fraction	9.9268×10^{-2}
feed temperature	343.15 K

reported on the convergence of the discrete numerical model to the mathematical model, as only the spatially converged cell-based model solution is shown.

To analyze the performance of the cell-based model, eight different configurations, as shown in Table 2, are defined. These configurations determine how the spatial discretization along the column height is performed. In addition to this macroscopic spatial dimension, along the liquid and vapor films, two mesoscopic dimensions must be discretized.

Figure 6 shows some liquid temperature profiles obtained for two different spatial discretizations along

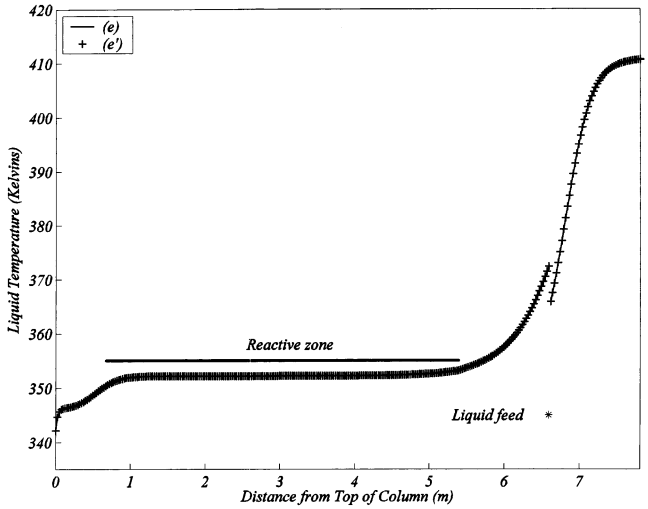

Figure 6. Liquid bulk temperature profiles for two configurations of the discrete model of the liquid−vapor interface. Sufficient discretization and convergence the discrete model of the liquid−vapor interface.

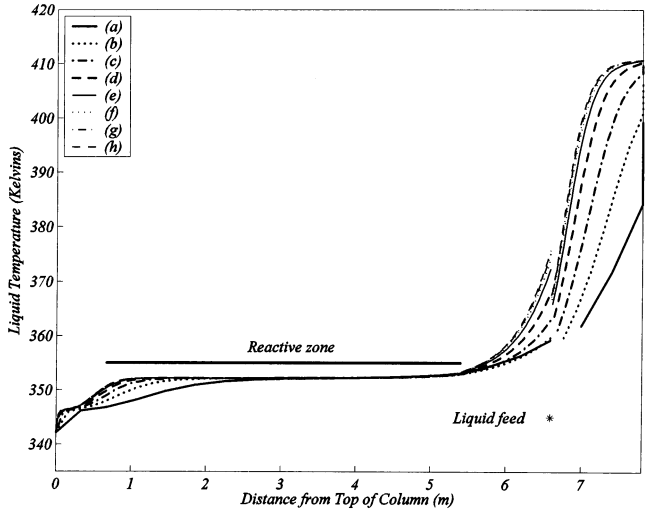

Figure 7. Liquid temperature profiles for different cell-based discrete models showing convergence of the cell-based models.

Table 2. Spatial Discretization Configurations (i.e., Number of Gridblocks in Each Section) for Cell-Based Models

	configuration							
	a	b	c	d	e	f	g	h
rectification	2	4	7	14	27	41	54	67
reactive	12	24	48	95	189	284	378	472
stripping (1)	3	6	12	24	48	72	96	120
stripping (2)	3	7	13	25	49	74	98	122
liquid film	4	4	4	4	4	4	4	4
vapor film	4	4	4	4	4	4	4	4

the two mesoscopic dimensions. The rectification, reactive, first stripping, and second stripping zones have 27, 189, 48, and 49 gridblocks, respectively. In each packed section, each gridblock has the same length. A cell approach is used along the column, whereas a higher-order scheme is employed for approximating the chemical processes inside the films. The difference between the two configurations is in the number of gridblocks in the liquid and vapor films. The first configuration, e′, has eight elements in each film, whereas the second configuration, e, has only four elements in each film. The two configurations exhibit the same behavior. Hence, only four gridblocks in each film are necessary.

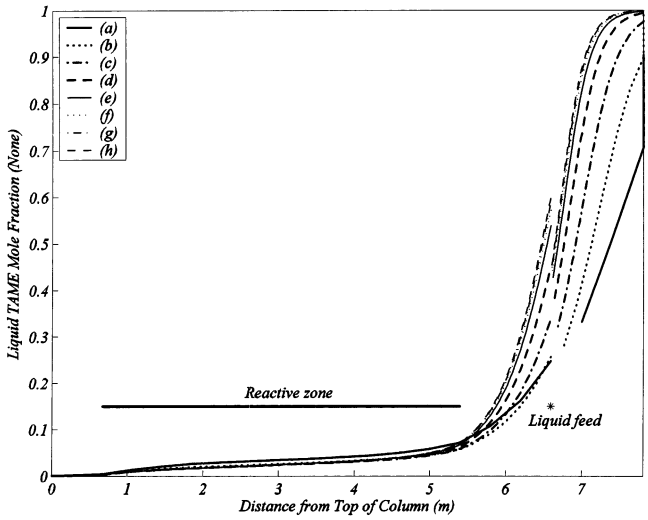

Figure 8. Liquid TAME mole fraction profiles for different cell-based discrete models showing convergence of the cell-based models.

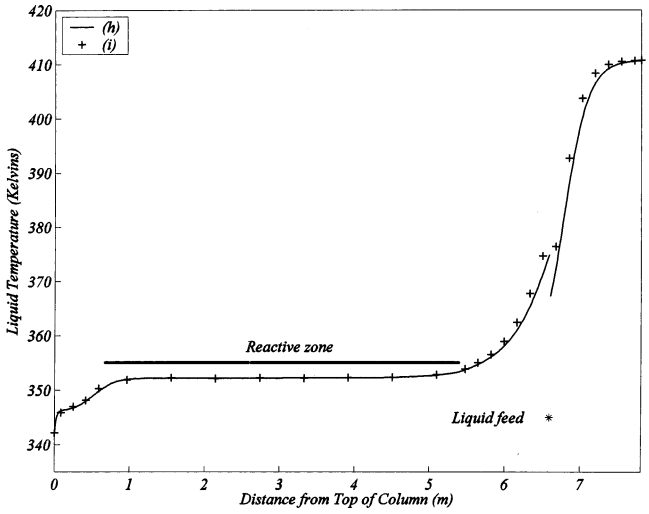

Figure 9. Liquid temperature profiles for the cell-based model versus the higher-order scheme.

Table 3. Conversions and Purities for Different Cell-Based Model Configurations

configuration	TAME purity	conversion
a	0.9041	0.3646
b	0.9718	0.4777
c	0.9934	0.5137
d	0.9985	0.5215
e	0.9994	0.5227
f	0.9996	0.5228
g	0.9997	0.5228
h	0.9997	0.5228

Therefore, from now on, the liquid−vapor interface is described using only four gridblocks in each the liquid and vapor films and the higher-order scheme.

The liquid temperature profiles (Figure 7) and the liquid TAME mole fraction profiles (Figure 8) for eight different configurations illustrate the extremely slow convergence of the cell-based approach. The largest model, denoted h, which has more than 250 000 variables, appears to have enough cells. Model e, which has more than 300 cells, has still not converged to the solution of the distributed-parameter model. A 300-cell rate-based model is already a large model that is rarely considered in case studies. Table 3 presents the conversion and purity for each of the eight configurations.

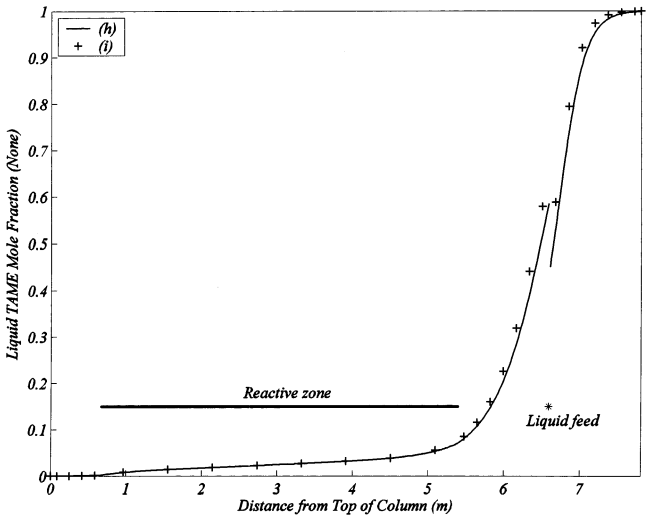

Figure 10. Liquid TAME mole fraction profiles for two cell-based models versus the higher-order scheme.

Table 4. Spatial Discretization Configurations (i.e., Number of Gridblocks in Each Section) for Higher-Order Discrete Model and Two Cell-Based Models

	model type and configuration		
	cell-based, a	cell-based, h	higher-order, i
rectification	2	67	4
reactive	12	472	8
stripping (1)	3	120	7
stripping (2)	3	122	7
liquid film	4	4	4
vapor film	4	4	4

Table 5. Key Numerical Properties for Cell-Based Models

configuration	number of variables	number of nonzero Jacobian elements	Jacobian density (%)
a	6804	40 736	0.087 993
b	13 518	82 361	0.045 071
c	26 004	159 836	0.023 637
d	50 966	314 686	0.012 115
e	100 576	622 461	0.006 154
f	151 138	936 111	0.004 098
g	200 748	1 243 886	0.003 087
h	250 358	1 551 661	0.002 476

Table 6. Key Numerical Properties for Higher-Order Scheme Discrete Models and Two Cell-Based Models

configuration	number of variables	number of nonzero Jacobian elements	Jacobian density (%)
a	6804	40 736	0.087993
h	250 358	1 551 661	0.002 476
i	8934	54 148	0.067 841

Table 7. Computation Times (s) for Cell-Based Models

configuration	converged solution	pressure (+5%)	total feed flow rate (+5%)	reflux ratio (+5%)	reflux ratio (+10%)
a	5	6.5	11	10	10
b	8	12	25	20	25
c	17	24	68	40	50
d	35	52	241	90	115
e	76	108	584	228	324
f	105	150	846	294	508
g	150	230	1650	479	1048
h	190	265	5770	645	1330

Usually, these properties are the characteristics that are used to design a column. Therefore, extreme caution is required when one intends to investigate a reactive distillation process through numerical simulations. A

Table 8. Computation Times (s) for Higher-Order Discrete Model and Two Cell-Based Models

configuration	model type	converged solution	pressure (+5%)	total feed flow rate (+5%)	reflux ratio (+5%)	reflux ratio (+10%)
a	cell-based	5	6.5	11	10	10
h	cell-based	190	265	5770	645	1330
i	higher-order	6	8	17	12	13

very large span of "solutions" can be obtained as the discretization level is refined. This is especially true for certain operating conditions.

A cell-based or first-order finite-difference method is commonly used for investigating reactive distillation processes. This strategy is particularly inefficient in converging to the solution of the mathematical model (Figures 7 and 8). Using a higher-order scheme such as that presented in section 3, the mathematical model of the packed reactive distillation column is solved easily with a discrete model of reduced size. The liquid temperature profiles (Figure 9) and the liquid TAME mole fraction profiles (Figure 10) illustrate the performance of the higher-order scheme. The configurations for these discrete models are shown in Table 4. The numerical results for discrete models h and i are very similar. However, the second configuration, i, which uses a higher-order scheme, leads to a discrete model of tractable size that can be used for model-based control strategies based on optimization.

The numerical properties of the discrete cell-based and higher-order models are comparable. The numerical implementation using the higher-order description of the mathematical model is not more complex than a cell-based method. The Jacobian matrices for configurations with the same number of gridblocks have similar densities and similar sparsity patterns for both methods. The minor differences lie in the approximation of the spatial derivatives. Table 5 reports some key numerical properties for the eight cell-based discrete models, whereas Table 6 lists these same properties for the configurations defined in Table 4. The dimension of the problem mainly scales with the number of gridblocks or cells.

The performance of the two methods in terms of computation time is assessed by solving the discrete models for different inputs. Taking a successful solution of a discrete model as the initial guess, a first time is recorded when no input is modified. Then, input changes in pressure, feed flow rate, and reflux ratio are executed, new solutions sought, and computation times are determined for each discrete model. For the cell-based model, the computation times are recorded in Table 7. Discrete models (cell-based and higher-order) having identical numbers of gridblocks require similar computational loads. However, to obtain a valid numerical solution of the distributed mathematical model, the cell-based approach performs poorly because it requires an extremely large number of gridblocks. In this case, a higher-order finite-difference discrete model significantly outperforms a cell-based model in term of computation time. This result is shown in Table 8. The computation times for higher-order discrete model i, which has 25 gridblocks, are similar to the times required for cell-based discrete model a, which has 20 cells. However, the discrete higher-order scheme has converged to a solution of the distributed mathematical model, whereas the cell-based model has not and would require about 700 cells to achieve the same accuracy.

5. Conclusions

In this paper, a general mathematical model and its numerical solution for packed reactive distillation is presented. The sets of equations and the underlying assumptions are briefly reviewed. Two different approaches are employed to obtain discrete models that approximate the general mathematical model. The cell-based approach is analyzed in a finite-difference framework, and its numerical weaknesses are identified. A higher-order finite-difference scheme is used to alleviate the difficulties encountered in the cell-based approach. Using a TAME-packed reactive distillation unit, the performances of the two methods are investigated. The higher-order scheme outperforms the cell-based approach. The higher-order scheme is numerically efficient and generates discrete models of tractable size suitable for control and optimization studies.

Acknowledgment

The Dot Products company provided the NOVA software. The authors thank Dr. Jeff Renfro for information regarding the use of NOVA. Dr. Kamy Sepehrnoori provided valuable assistance on finite-difference methods and numerical issues. Financial support from AspenTech is also acknowledged.

Nomenclature

A_c = column cross-sectional area (m^2)
a_e = specific effective liquid−vapor interfacial area (m^2 interfacial area/m^3 packing)
C = spatial dependent variable or function
d'_j = driving force (m^{-1})
d_j = dimensionless driving force
$d_{a\rightarrow z}$ = displacement between position a and position z (m)
$Đ_{j,k}$ = Maxwell−Stefan diffusivity coefficient (m^2/s)
dz = differential increment (m)
H = enthalpy (J/kmol)
H_j = partial molar enthalpy (J/kmol)
h = heat-transfer coefficient [J/(s m^2 K)]
K_j = equilibrium constant
L_H = liquid energy flow rate (J/s)
L_j = liquid molar flow rate (kmol/s)
L_T = total liquid molar flow rate (kmol/s)
l_s = section length (m)
M_H = energy holdup (J)
M_j = molar holdup (kmol)
M_T = total molar holdup (kmol)
N = number of gridblocks in a section
N_{1nr} = number of gridblocks in nonreactive zone 1
N_{2nr} = number of gridblocks in nonreactive zone 2
N_{3nr} = number of gridblocks in nonreactive zone 3
N_{1rc} = number of gridblocks in reactive zone 1
N_{comp} = number of components
N_{lfm} = number of gridblocks in liquid film
N_{vfm} = number of gridblocks in vapor film
n_H = energy flux across the interface from vapor to liquid ($J/s/m^2$)
n_j = material flux across the interface from vapor to liquid ($kmol/s/m^2$)
P = pressure (Pa)

ΔP = pressure drop (Pa/m)
Q_{Loss} = heat loss [J/(s m) or J/s]
Q_C = cooling duty (J/s)
r_j = reaction rate [kmol/(s kg of catalyst)]
t = time (s)
T = temperature (K)
U_H = energy holdup (J/m)
U_j = molar holdup (kmol/m)
U_T = total molar holdup (kmol/m)
V_H = vapor energy flow rate (J/s)
V_j = vapor molar flow rate (kmol/s)
V_T = total vapor molar flow rate (kmol/s)
Vol = vessel volume (m^3)
x = vector of liquid mole fractions
x_j = component liquid mole fraction
y = vector of vapor mole fractions
y_j = component vapor mole fraction
z = axial section position (m)
Δz_i = gridblock size (m)
z^{lf} = liquid-film position
z^{vf} = vapor-film position

Greek Letters

α_i = coefficient for gridblock i
α_i' = coefficient for gridblock i (m^{-1})
β_i = coefficient for gridblock i
β_i' = coefficient for gridblock i (m^{-1})
γ_i = coefficient for gridblock i
γ_i' = coefficient for gridblock i (m^{-1})
δ_i = coefficient for gridblock i
δ_i' = coefficient for gridblock i (m^{-1})
ϵ = void fraction (m^3 available to bulk phases/m^3 of packing)
$\kappa_{j,k}$ = mass-transfer coefficient (m/s)
λ = thermal conductivity [J/(s m K)]
ν = viscosity [kg/(s m)]
ρ = molar density (kmol/m^3)
σ = surface tension (N/m)
Φ = volume fraction of a bulk phase (m^3 of bulk phase/m^3 of packing)
ω_c = catalyst density (kg of catalyst/m^3 of packing)

Subscripts

H = energy
i = gridblock index
j = component index
k = component index
l = integer index
T = total

Superscripts

Atm = atmosphere
L = liquid phase
lb = liquid bulk phase
lf = liquid film
V = vapor phase
vb = vapor bulk phase
vf = vapor film
vl = vapor to liquid

Abbreviations

2M1B = 2-methyl-1-butene
2M2B = 2-methyl-2-butene
TAME = *tert*-amyl methyl ether

Appendix A

In this section, additional equations required to fully model a packed reactive distillation column are presented. First, a set of relations for completing the description of the macroscopic behavior of a packed zone are listed.

$$U_j^{lb} - U_T^{lb} x_j^{lb} = 0 \quad \text{(A-1)}$$

$$U_j^{vb} - U_T^{vb} y_j^{vb} = 0 \quad \text{(A-2)}$$

$$U_H^{lb} - U_T^{lb}(H^{lb} - P/\rho^{lb}) = 0 \quad \text{(A-3)}$$

$$U_H^{vb} - U_T^{vb}(H^{vb} - P/\rho^{vb}) = 0 \quad \text{(A-4)}$$

$$L_j^{lb} - L_T^{lb} x_j^{lb} = 0 \quad \text{(A-5)}$$

$$V_j^{vb} - V_T^{vb} y_j^{vb} = 0 \quad \text{(A-6)}$$

$$L_H^{lb} - L_T^{lb} H^{lb} = 0 \quad \text{(A-7)}$$

$$V_H^{vb} - V_T^{vb} H^{vb} = 0 \quad \text{(A-8)}$$

$$L_T^{lb} - \sum_{j=1}^{N_{comp}} L_j^{lb} = 0 \quad \text{(A-9)}$$

$$V_T^{vb} - \sum_{j=1}^{N_{comp}} V_j^{vb} = 0 \quad \text{(A-10)}$$

Equations A-1−A-10 are usually called constitutive relations and are required for describing the links between the molar flow rates and the molar holdups: these variables share some intensive properties (x^{lb}, y^{lb}, H^{lb}, H^{vb}). An additional group of equations consists of physical and thermodynamic properties (eqs A-11−A-17). Relations A-11 and A-12 determine the temperatures of the bulk phases. The physical and thermodynamic models are part of the mathematical model. Different physical and thermodynamic properties can be implemented. Only the functionals defining these properties are modified; the overall structure of the model remains identical.

$$H^{lb} - f_{\text{liquid enthalpy}}(x^{lb}, T^{lb}) = 0 \quad \text{(A-11)}$$

$$H^{vb} - f_{\text{vapor enthalpy}}(y^{vb}, T^{vb}, P) = 0 \quad \text{(A-12)}$$

$$\rho^{lb} - f_{\text{liquid molar density}}(x^{lb}, T^{lb}) = 0 \quad \text{(A-13)}$$

$$\rho^{vb} - f_{\text{vapor molar density}}(y^{vb}, T^{vb}, P) = 0 \quad \text{(A-14)}$$

$$\nu^{lb} - f_{\text{liquid viscosity}}(x^{lb}, T^{lb}) = 0 \quad \text{(A-15)}$$

$$\nu^{vb} - f_{\text{vapor viscosity}}(y^{vb}, T^{vb}) = 0 \quad \text{(A-16)}$$

$$\sigma - f_{\text{surface tension}}(x^{lb}, T^{lb}) = 0 \quad \text{(A-17)}$$

A last set of equations used in describing the macroscopic behavior of a packed section consists of relations representing operating constraints (eqs A-18−A-24). The first two equations of this group (eqs A-18 and A-19) define the total molar holdups as a function of the operating conditions. Equation A-20 is an empirical relation that expresses the volume fraction of liquid per unit volume of packing. This group ends the set of equations that describe the macroscopic behavior of a reactive section. In a nonreactive section, the reaction terms are set to zero.

$$U_T^{lb} - \Phi^{lb} A_c \rho^{lb} = 0 \quad \text{(A-18)}$$

$$U_T^{vb} - \Phi^{vb} A_c \rho^{vb} = 0 \quad \text{(A-19)}$$

$$\Phi^{lb} - f_{\text{liquid fraction}}(L_T^{lb}, \rho^{lb}, \rho^{vb}, \Delta P, \Phi^{lb}, \nu^{lb}, \sigma, x^{lb}, y^{vb}) = 0 \quad \text{(A-20)}$$

$$\Phi^{vb} + \Phi^{lb} - \epsilon = 0 \quad \text{(A-21)}$$

$$a_e - f_{\text{effective surface area}}(L_T^{lb}, \rho^{lb}, \nu^{lb}, \sigma, x^{lb}) = 0 \quad \text{(A-22)}$$

$$Q_{\text{Loss}}^{lb} - f_{\text{liquid heat loss}}(T^{lb}, T^{Atm}) = 0 \quad \text{(A-23)}$$

$$Q_{\text{Loss}}^{vb} - f_{\text{vapor heat loss}}(T^{lb}, T^{Atm}) = 0 \quad \text{(A-24)}$$

The description of the rate-based processes occurring inside the liquid and vapor films requires additional equations. The following relations complete the set of equations presented in section 2.3. This large set of equations used in describing the phenomena occurring between the two bulk phases consists of relations describing physical, thermodynamic, and transport properties. The Maxwell−Stefan diffusivities (eqs A-25 and A-26), the binary mass-transfer coefficients (eqs A-27 and A-28), the heat-transfer coefficients (eqs A-29 and A-30), the partial molar enthalpies (eqs A-31 and A-32), the thermal conductivities (eqs A-33 and A-34), and the molar densities (eqs A-35 and A-36) are required properties that need to be evaluated for the differential equations defined by the Maxwell−Stefan relations to be integrated.

$$Đ_{j,k}^{lf} - f_{j,k\ \text{liquid Maxwell−Stefan diffusivities}}(x^{lf}, T^{lf}) = 0 \quad \text{(A-25)}$$

$$Đ_{j,k}^{vf} - f_{j,k\ \text{vapor Maxwell−Stefan diffusivities}}(T^{vf}, P) = 0 \quad \text{(A-26)}$$

$$\kappa_{j,k}^{lf} - f_{j,k\ \text{liquid mass transfer coefficients}}(L_T^{lb}, \Phi^{lb}, \rho^{lb}, Đ_{j,k}^{lf}) = 0 \quad \text{(A-27)}$$

$$\kappa_{j,k}^{vf} - f_{j,k\ \text{vapor mass transfer coefficients}}(y^{vf}, V_T^{vb}, L_T^{lb}, \Phi^{lb}, \rho^{vb}, \rho^{lb}, \nu^{vb}, Đ_{j,k}^{vf}) = 0 \quad \text{(A-28)}$$

$$h^{lf} - f_{\text{liquid heat transfer coefficient}}(x^{lf}, T^{lf}, L_T^{lb}, \Phi^{lb}, \rho^{lb}, \nu^{lb}, Đ_{j,k}^{lf}, \kappa_{j,k}^{lf}, \lambda^{lf}) = 0 \quad \text{(A-29)}$$

$$h^{vf} - f_{\text{vapor heat transfer coefficient}}(y^{vf}, T^{vf}, V_T^{vb}, \Phi^{vb}, \rho^{vb}, \nu^{vb}, Đ_{j,k}^{vf}, \kappa_{j,k}^{vf}, \lambda^{vf}) = 0 \quad \text{(A-30)}$$

$$H_j^{lf} - f_{j\ \text{liquid partial molar enthalpy}}(x^{lf}, T^{lf}) = 0 \quad \text{(A-31)}$$

$$H_j^{vf} - f_{j\ \text{vapor partial molar enthalpy}}(y^{vf}, T^{vf}, P) = 0 \quad \text{(A-32)}$$

$$\lambda^{lf} - f_{\text{liquid conductivity}}(x^{lf}, T^{lf}) = 0 \quad \text{(A-33)}$$

$$\lambda^{vf} - f_{\text{vapor conductivity}}(y^{vf}, T^{vf}) = 0 \quad \text{(A-34)}$$

$$\rho^{lf} - f_{\text{liquid molar density}}(x^{lf}, T^{lf}) = 0 \quad \text{(A-35)}$$

$$\rho^{vf} - f_{\text{vapor molar density}}(y^{vf}, T^{vf}, P) = 0 \quad \text{(A-36)}$$

The following set of algebraic equations is used to fully model the partial condenser.

$$M_j^L + M_j^V - M_j^T = 0 \quad \text{(A-37)}$$

$$M_H^L + M_H^V - M_H^T = 0 \quad \text{(A-38)}$$

$$M_j^L - x_j M_T^L = 0 \quad \text{(A-39)}$$

$$M_H^L - M_T^L (H^L - P/\rho^L) = 0 \quad \text{(A-40)}$$

$$H^L - f_{\text{liquid enthalpy}}(x, T^L) = 0 \quad \text{(A-41)}$$

$$\rho^L - f_{\text{liquid molar density}}(x, T^L) = 0 \quad \text{(A-42)}$$

$$\sum_{j=1}^{N_{comp}} M_j^L - M_T^L = 0 \quad \text{(A-43)}$$

$$\text{Vol}^L - \rho^L M_T^L = 0 \quad \text{(A-44)}$$

$$L_T^{Condenser} - f_{\text{Condenser}}^L(\rho^L, M_T^L) = 0 \quad \text{(A-45)}$$

$$L_j^{Condenser} - x_j L_T^{Condenser} = 0 \quad \text{(A-46)}$$

$$L_H^{Condenser} - H^L L_T^{Condenser} = 0 \quad \text{(A-47)}$$

$$M_j^V - y_j M_T^V = 0 \quad \text{(A-48)}$$

$$M_{Inert}^V - M_{Inert}^T = 0 \quad \text{(A-49)}$$

$$M_H^V - M_T^V (H^V - P/\rho^V) = 0 \quad \text{(A-50)}$$

$$y_j - K_j x_j = 0 \quad \text{(A-51)}$$

$$M_{Inert}^V - y_{Inert} M_V^T = 0 \quad \text{(A-52)}$$

$$H^V - f_{\text{vapor enthalpy}}(y, y_{\text{Inert}}, T^V, P) = 0 \quad \text{(A-53)}$$

$$T^L - T^V = 0 \quad \text{(A-54)}$$

$$\text{Vol}^V - \rho^V M_T^V = 0 \quad \text{(A-55)}$$

$$\sum_{j=1}^{N_{comp}} M_j^V + M_{Inert}^V - M_T^V = 0 \quad \text{(A-56)}$$

$$\text{Vol}^L + \text{Vol}^V - \text{Vol}^{Condenser} = 0 \quad \text{(A-57)}$$

$$V_T^{Condenser} - f_{\text{Condenser}}^V(P^{\text{Reflux drum}}, P) = 0 \quad \text{(A-58)}$$

$$V_j^{Condenser} - y_j V_T^{Condenser} = 0 \quad \text{(A-59)}$$

$$V_{Inert}^{Condenser} - y_{Inert} V_T^{Condenser} = 0 \quad \text{(A-60)}$$

$$V_H^{Condenser} - H^V V_T^{Condenser} = 0 \quad \text{(A-61)}$$

The last set of equations for the mathematical model of the condenser contains a relation for fixing the pressure of the vessel (eq A-62), an equation specifying the cooling duty (eq A-63), and an equation defining the total energy loss for the condenser (eq A-64), as well as an equation describing the liquid−vapor equilibrium (eq A-65).

$$\rho^v - f_{\text{vapor molar density}}(y, y_{\text{Inert}}, T^V, P) = 0 \quad \text{(A-62)}$$

$$Q_C - \text{input} = 0 \quad \text{(A-63)}$$

$$Q^{T}_{Loss} - f_{\text{total heat loss}}(T^{L}, T^{Atm}) = 0 \quad \text{(A-64)}$$

$$K_j - f_{j\ \text{equilibrium constant}}(x, y, y_{Inert}, T^{L}, P) = 0 \quad \text{(A-65)}$$

Equation A-63 sets an operating condition. In the proposed model, the cooling duty is fixed.

The last set of algebraic equations is related to the modeling of the reflux drum and completes the differential equations briefly presented in section 2.4.3. The liquid phase is defined according to a set of variables similar to that used for the liquid phase of the condenser. The mole fractions, enthalpy, temperature, and molar density (intensive variables) are determined through eqs A-66−A-69.

$$M^{L}_{j} - x_j M^{L}_{T} = 0 \quad \text{(A-66)}$$

$$M^{L}_{H} - M^{L}_{T}(H^{L} - P/\rho^{L}) = 0 \quad \text{(A-67)}$$

$$H^{L} - f_{\text{liquid enthalpy}}(x, T^{L}) = 0 \quad \text{(A-68)}$$

$$\rho^{L} - f_{\text{liquid molar density}}(x, T^{L}) = 0 \quad \text{(A-69)}$$

The liquid total molar holdup and its volume, which are extensive variables, are computed using eqs A-70 and A-71.

$$\sum_{j=1}^{N_{comp}} M^{L}_{j} - M^{L}_{T} = 0 \quad \text{(A-70)}$$

$$\text{Vol}^{L} - \rho^{L} M^{L}_{T} = 0 \quad \text{(A-71)}$$

The liquid streams leaving the reflux drum are defined by eqs A-72−A-77. The heat loss that occurs from the liquid phase is fixed according to eq A-78.

$$L^{Distillate}_{T} - \text{input} = 0 \quad \text{(A-72)}$$

$$L^{Distillate}_{j} - x_j L^{Distillate}_{T} = 0 \quad \text{(A-73)}$$

$$L^{Distillate}_{H} - H^{L} L^{Distillate}_{T} = 0 \quad \text{(A-74)}$$

$$L^{Reflux}_{T} - \text{input} = 0 \quad \text{(A-75)}$$

$$L^{Reflux}_{j} - x_j L^{Reflux}_{T} = 0 \quad \text{(A-76)}$$

$$L^{Reflux}_{H} - H^{L} L^{Reflux}_{T} = 0 \quad \text{(A-77)}$$

$$Q^{T}_{Loss} - f^{L}_{Heatloss}(T^{L}, T^{Atm}) = 0 \quad \text{(A-78)}$$

The vapor bulk phase is modeled in a similar fashion: A set of relations defines intensive variables (eqs A-79−A-83) and then extensive variables are fixed (eqs A-84−A-85). Finally, the vapor streams are determined. For each stream, an equation determines the total molar flow rate, and then the material and energy flow rates are defined. First, the outlets leaving the reflux drum are modeled. Two outlet streams exist: a vent stream and a connection to the condenser (eqs A-86−A-93). The vapor inert inlet entering the reflux drum to control the pressure is eventually modeled as a stream defined by a set of equations that fixes its total molar flow rate (input) and its energy flow rate, eqs A-94−A-96. The last equation of this set defines the heat loss for the vapor phase (eq A-97).

$$M^{V}_{j} - y_j M^{V}_{T} = 0 \quad \text{(A-79)}$$

$$M^{V}_{Inert} - y_{Inert} M^{V}_{T} = 0 \quad \text{(A-80)}$$

$$M^{V}_{H} - M^{V}_{T}(H^{V} - P/\rho^{V}) = 0 \quad \text{(A-81)}$$

$$H^{V} - f_{\text{vapor enthalpy}}(y, y_{Inert}, T^{V}, P) = 0 \quad \text{(A-82)}$$

$$\text{Vol}^{V} - \rho^{V} M^{V}_{T} = 0 \quad \text{(A-83)}$$

$$\sum_{j=1}^{N_{comp}} M^{V}_{j} + M^{V}_{Inert} - M^{V}_{T} = 0 \quad \text{(A-84)}$$

$$\text{Vol}^{L} + \text{Vol}^{V} - \text{Vol}^{\text{Reflux drum}} = 0 \quad \text{(A-85)}$$

$$V^{\text{Reflux drum}}_{T} - f^{V}_{Refluxdrum}(P^{\text{Condenser}}, P) = 0 \quad \text{(A-86)}$$

$$V^{\text{Reflux drum}}_{j} - y_j V^{\text{Reflux drum}}_{T} = 0 \quad \text{(A-87)}$$

$$V^{\text{Reflux drum}}_{Inert} - y_{Inert} V^{\text{Reflux drum}}_{T} = 0 \quad \text{(A-88)}$$

$$V^{\text{Reflux drum}}_{H} - H^{V} V^{\text{Reflux drum}}_{T} = 0 \quad \text{(A-89)}$$

$$V^{Vent}_{T} - f^{V}_{Vent}(P, \text{input}) = 0 \quad \text{(A-90)}$$

$$V^{Vent}_{j} - y_j V^{Vent}_{T} = 0 \quad \text{(A-91)}$$

$$V^{Vent}_{Inert} - y_{Inert} V^{Vent}_{T} = 0 \quad \text{(A-92)}$$

$$V^{Vent}_{H} - H^{V} V^{Vent}_{T} = 0 \quad \text{(A-93)}$$

$$V^{Inert} - \text{input} = 0 \quad \text{(A-94)}$$

$$V^{Inert}_{H} - H^{Inert} V^{Inert} = 0 \quad \text{(A-95)}$$

$$H^{Inert} - f_{\text{inert enthalpy}}(T^{Inert}, P) = 0 \quad \text{(A-96)}$$

$$Q^{V}_{Loss} - f^{V}_{Heatloss}(T^{V}, T^{Atm}) = 0 \quad \text{(A-97)}$$

The final equation of the model determines the pressure for the entire reflux drum.

$$\rho^{V} - f_{\text{vapor molar density}}(y, y_{Inert}, T^{V}, P) = 0 \quad \text{(A-98)}$$

Appendix B

The liquid molar density is computed by a modified Rackett model,[19] whereas the ideal gas law is used to describe the vapor molar density. The liquid viscosity of the mixture is evaluated through a product-mixing rule; for the vapor, the Reichenberg method is used.[19] The pure-component surface tensions come from the DIPPR database.[20] A molar-average mixing rule is used for computing the surface tension of the mixture. The liquid conductivity of the mixture is the molar average of pure-component liquid conductivities obtained from the Chemical Properties Handbook.[21] The same method is used for the vapor phase. The heat-transfer coefficients, which are required for the interface models, are evaluated using the Chilton−Colburn analogy.[10] The

liquid interdiffusion coefficients in dilute solutions for each binary pair are evaluated using the Wilke−Chang method.[22] The Maxwell−Stefan diffusivities for each pair are then computed through the rules presented by Kooijman and Taylor.[10] For the vapor phase, the Chapman−Enskog model defines the Maxwell−Stefan diffusivities, assuming ideal behavior. The mass-transfer coefficients for the liquid and vapor films are evaluated with the packing relations proposed by Rocha et al.[18] The dimensionless driving forces for molar diffusion (d_j) used in the Maxwell−Stefan relations are computed with the UNIQUAC model for the liquid phase as presented by Taylor and Krishna.[10] Ideal behavior is assumed in the vapor film, so the dimensionless driving forces are reduced to vapor mole fraction gradients inside the vapor film. Ideal liquid and vapor enthalpies as well as ideal partial molar enthalpies are used. The models are from the DIPPR database.[20]

Literature Cited

(1) Taylor, R.; Krishna, R. Review of Modelling Reactive Distillation. *Chem. Eng. Sci.* **2000**, *55*, 5183.

(2) Baur, R.; Higler, A.; Taylor, R.; Krishna, R. Comparison of Equilibrium Stage and Nonequilibrium Stage Models for Reactive Distillation. *Chem. Eng. J.* **1999**, *76*, 33.

(3) Baur, R.; Taylor, R.; Krishna, R. Dynamic Behavior of Reactive Distillation Columns Described by a Nonequilibrium Stage Model. *Chem. Eng. Sci.* **2001**, *56*, 2085.

(4) Higler, A.; Krishna, R.; Taylor, R. A. Nonequilibrium Cell Model for Multicomponent (Reactive) Separation Processes. *American Institute of Chem. Eng. J.* **1999**, *45*, 2357.

(5) Kreul, L. U.; Górak, A.; Barton, P. I. Modeling of Homogeneous Reactive Separation Processes in Packed Columns. *Chem. Eng. Sci.* **1999**, *54*, 19.

(6) Schneider, R.; Noeres, C.; Kreul, L. U.; Górak, A. Dynamic Modeling and Simulation of Reactive Batch Distillation. *Comput. Chem. Eng.* **2001**, *25*, 169.

(7) Kreul, L. U. Discontinuous and Reactive Distillation. Ph.D. Thesis, University of Dortmund, Dortmund, Germany, 1998.

(8) Sundmacher, K.; Hoffmann, U. Development of a New Catalytic Distillation Process for Fuel Ethers via a Detailed Nonequilibrium Model. *Chem. Eng. Sci.* **1996**, *51*, 2359.

(9) Kreul, L. U.; Górak, A.; Dittrich, C.; Barton, P. I. Dynamic Catalytic Distillation: Advanced Simulation and Experimental Validation. *Comput. Chem. Eng.* **1998**, *22*, S371.

(10) Taylor, R.; Krishna, R. *Multicomponent Mass Transfer*; Wiley: New York, 1993.

(11) Finlayson, B. A. *The Method of Weighted Residuals and Variational Principles*; Academic Press: New York, 1972.

(12) Liu, J.; Pope, G. A.; Sepehrnoori, K. A High-Resolution Finite-Difference Scheme for Nonuniform Grids. *Appl. Math. Modell.* **1995**, *19*, 162.

(13) Liu, J.; Delshad, M.; Pope, G. A.; Sepehrnoori, K. Application of Higher-Order Flux-Limited Methods in Compositional Simulation. *Transp. Porous Media* **1994**, *16*, 1.

(14) Allgower, E. L.; Georg, K. *Numerical Continuation Methods—An Introduction*; Springer-Verlag: Berlin, 1990.

(15) Rihko, L. K.; Krause, A. O. I. Kinetics of Heterogeneously Catalyzed *tert*-Amyl Methyl Ether Reactions in the Liquid Phase. *Ind. Eng. Chem. Res.* **1995**, *34*, 1172.

(16) Rihko, L. K.; Kiviranta-Pääkkönen, P. K.; Krause, A. O. I. Kinetic Model for the Etherification of Isoamylenes with Methanol. *Ind. Eng. Chem. Res.* **1997**, *36*, 614.

(17) Rocha, J. A.; Bravo, J. L.; Fair, J. R. Distillation Columns Containing Structured Packings: A Comprehensive Model for Their Performance. 1. Hydraulic Models. *Ind. Eng. Chem. Res.* **1993**, *32*, 641.

(18) Rocha, J. A.; Bravo, J. L.; Fair, J. R. Distillation Columns Containing Structured Packings: A Comprehensive Model for Their Performance. 2. Mass-Transfer Model. *Ind. Eng. Chem. Res.* **1996**, *35*, 1660.

(19) Poling, B. E.; Prausnitz, J. M.; O'Connel, J. P. *The Properties of Gases and Liquids*; MacGraw-Hill: New York, 2001.

(20) *Physical and Thermodynamic Properties of Pure Chemicals DIPPR Project 801 Evaluated Process Design Data*; Taylor & Francis: Philadelphia, PA, 1999.

(21) Yaws, C. L. *Chemical Properties Handbook*; MacGraw-Hill: New York, 1999.

(22) Hines, A. L.; Maddox, R. N. *Mass Transfer Fundamentals and Applications*; Prentice Hall, Inc.: Englewood Cliffs, NJ, 1985.

Received for review February 26, 2003
Revised manuscript received January 21, 2004
Accepted January 22, 2004

IE030171N